ChemComm

COMMUNICATION

View Article Online
View Journal | View Issue

Cite this: *Chem. Commun.*, 2015, **51**, 3117

Received 6th November 2014,
Accepted 6th January 2015

DOI: 10.1039/c4cc08876j

www.rsc.org/chemcomm

A patterned ZnO nanorod array/gas sensor fabricated by mechanoelectrospinning-assisted selective growth†

Xiaomei Wang,[a] Fazhe Sun,[b] Yongan Huang,*[a] Yongqing Duan[a] and Zhouping Yin*[a]

Micropatterned ZnO nanorod arrays were fabricated by the mechanoelectrospinning-assisted direct-writing process and the hydrothermal growth process, and utilized as gas sensors that exhibited excellent Ohmic behavior and sensitivity response to oxidizing gas NO_2 at low concentrations (1–100 ppm).

Zinc oxide (ZnO) is a typical n-type direct wide band gap (3.37 eV) and large excitation binding energy (60 MeV) semiconductor, and it plays an important role in many fields ranging from optoelectronics to energy conversion, photocatalysis, photodectors, and nanosensors.[1–3] One-dimensional ZnO nanostructure has attracted much attention owing to its extensive applications in light-emitting diodes,[4,5] thin film transistors,[6] field-effect transistors,[3,7] chemical sensors,[7] piezoelectric sensors[8] and solar cells.[9]

The synthesis of ZnO nanostructures has been carried out using various methods, such as aqueous electrodeposition,[10] thermal evaporation and condensation,[11] physical/chemical vapor deposition,[4,12] solvothermal methods[13] and hydrothermal methods.[14] Among these methods, the hydrothermal method has been considered as an excellent procedure for the preparation of crystalline nanomaterials due to its low-cost, low temperature, simple process control, environmentally friendly nature. In nanodevices, it is significant to realize patterned and aligned ZnO nanorods, representing more integrated applications. Instead of randomly distributed nanorods on a substrate, an effective method is to selectively grow nanostructures directly on the desired areas of the substrate. Generally, the technique utilized to achieve a site-specific growth of ZnO nanorods involves micropatterning of the precursor and selective growth. It is hard to find suitable etching conditions in ceramic thin films to obtain patterned ZnO nanorods. Various methods for ZnO micropattern preparation have been reported, such as ink-jet printing,[15–17] self-assembled monolayers,[18] microcontact printing,[19] nanoimprint lithography,[20] pulsed laser deposition[21] and photolithography.[22] However, these approaches are limited by high temperature treatment, high vacuum systems, lithography or complication of the process and the need for a mask or a mold.

This work presents a mechanoelectrospinning (MES)-assisted selective growth technique to fabricate a patterned ZnO nanorod array/gas sensor. It utilizes a MES direct-writing method[23,24] to deposit the fiber-lattices of the precursor. MES adopts a short nozzle-to-substrate distance to improve positioning of the electrospun fibers of the ZnAc precursor. The diameter and position of the deposited fiber can be controlled over a large-area substrate in a direct, continuous manner. This method can fabricate orderly nanofibers continuously with a high local positioning accuracy. The combination of the MES method and the low-temperature hydrothermal method is presented for selectively growing ZnO nanorods. By tuning the printing conditions and the hydrothermal reaction time, the aligned arrays of ZnO nanorods with tunable spacing/diameter, uniform morphology and good crystal quality can be achieved. Finally, the ZnO nanorod array on the alumina substrate with an interdigital electrode is exposed to oxidizing gas NO_2[25] at low concentrations at 225 °C. It is indicated that the ZnO sample has good Ohmic behavior and high response to NO_2. The patterned ZnO parallel array is more easily integrated with other functional materials or electronic devices than the ZnO film of randomly distributed nanorods for gas sensing. The presented technique can fabricate a patterned ZnO nanorod array/gas sensor in a direct, low-cost, low-temperature, template-free, and highly controllable manner.

The experimental setup of MES is shown in Fig. 1(a). The MES process needs two electrodes: (1) a stainless steel nozzle is adopted as one electrode, connecting a high voltage DC power supplier and a syringe pump; and (2) another electrode is the ground collector which is fixed on the X–Y moving stage. The substrate is mounted on the ground collector underneath the nozzle. The nozzle-to-substrate distance ranges from 2–5 mm, which is much shorter than conventional electrospinning. A high-speed camera is used to observe the dynamic process of the jet.

[a] *State Key Laboratory of Digital Manufacturing Equipment and Technology, Huazhong University of Science and Technology, Wuhan 430074, China. E-mail: yahuang@hust.edu.cn, yinzhp@mail.hust.edu.cn*

[b] *Analysis Testing Center, Shandong University of Technology, Zibo 255100, China*

† Electronic supplementary information (ESI) available: Materials and equipment, ZnAc seed layer synthesis and ZnO nanorod selective growth, and characterization. See DOI: 10.1039/c4cc08876j

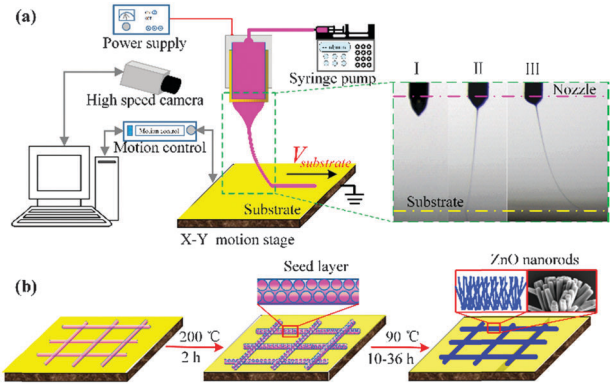

Fig. 1 (a) Schematic diagram of the MES setup. I, II and III are the images of the jet in different stages indicated by the dashed line box. (b) Growth process of the directly patterned ZnO nanorod array.

An aqueous solution containing zinc acetate (ZnAc) and polyethylene oxide (PEO) is fabricated by magnetic stirring. Initially, the nozzle shown in Fig. 1(a) is filled with ZnAc precursor solution. When 1.5–2.75 kV voltage and 450–900 nl min^{-1} flow rate are applied, the solution is sucked out from the needle, attaches to the nozzle orifice, and forms the Taylor cone at the apex of the nozzle (Fig. 1(a) I). Then the applied voltage increases gradually up to the onset voltage. As the electrostatic force is sufficient to overcome the surface tension of the sucked solution, a thin jet ejects from the apex of the Taylor cone, and forms a fiber between the nozzle and the substrate (Fig. 1(a) II). Then, the applied voltage is reduced gradually and appropriately just to keep the jet stable. The liquid jet undergoes extensive stretching forming linear fibers on the substrate orderly by the mechanical drawing force in one direction (Fig. 1(a) III). Meanwhile, the jet diameter becomes controllable due to the mechanical drawing force resulting from the digitally controllable high-speed motion.[26,27]

The hydrothermal growth of the ZnO nanorod array was carried out in three steps. An aqueous solution containing PEO makes electrospinning easier and ZnAc was directly written on the Si substrate by MES. Then the obtained samples were annealed at 200 °C for 2 hours to form ZnAc nanoparticle nuclei and to ensure that the seed particle adhesion to the substrate formed the seed layer. Finally, direct patterned ZnO nanorod arrays were selectively grown from ZnAc nanoparticle nuclei through hydrothermal growth (see ESI†). The schematic representation of the whole experimental process is shown in Fig. 1(b).

To fabricate the two-dimensional orthogonal microstructure of a large-area, well-defined ZnAc array (Fig. 2(a)), a parallel array of ZnAc and PEO was first directly written along one direction, and then along the perpendicular direction. The samples of the parallel and orthogonal arrays of ZnAc and PEO were annealed to fabricate ZnAc nanoparticle nuclei as the seed layer. The ZnO nanorod array was grown by subsequent selective hydrothermal growth. Fig. 2(b) and (c) show the field emission scanning electron microscope (SEM) images of parallel and orthogonal arrays of ZnO nanorods, respectively. High-density, radially grown, flower-type structures are shown in the insets of Fig. 2(b) and (c). The width of the flower-like structure is about 20 μm, and the distributions are uniform. Additionally, the ZnO nanorods originated from the center of the flower are randomly

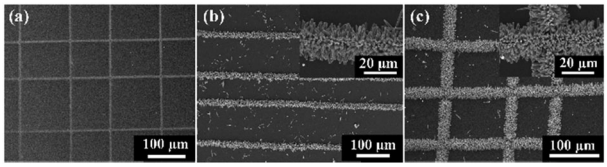

Fig. 2 (a) Low magnified SEM image of patterned ZnAc–PEO arrays on the Si substrate by MES; the ZnO nanorod array by subsequent selective hydrothermal growth, (b) parallel array, and (c) orthogonal array; the insets are high magnification SEM images of a parallel array and an orthogonal array, respectively.

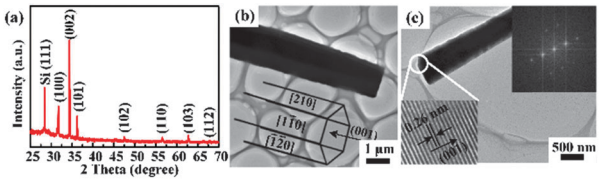

Fig. 3 (a) XRD patterns of ZnO nanorods growing for 12 h. (b and c) TEM images of single nanorods growing for 12 h; the bottom left inset in (c) is the HR-TEM image of the area indicated by the white circle, and the upper right inset image represents the SAED pattern of ZnO.

grown in all directions. In fact, the central part of the flower-shape structure corresponding to ZnO seed particle nuclei formed on the substrate provides a root for the growth of the ZnO nanorods.

Typical X-ray diffraction (XRD) patterns of ZnO nanorods are shown in Fig. 3(a). All the diffraction peaks are well indexed to the standard diffraction pattern of hexagonal phase ZnO with lattice constants of a = 0.3249 nm and c = 0.5206 nm (JCPDS card no. 36-1451). The grown structure is c-axis oriented. In addition, in comparison with the standard XRD pattern, the intensity ratio of the (002) to (101) diffraction peak which is the usual maximum reflection increases significantly, indicating that (001) is the relatively preferred growth direction of the structure, and the orientation of ZnO nanorods is further improved. Moreover, there is a Si peak at 28.37° owing to the existence of the Si substrate. The sharp diffraction peaks representing the narrow spectral width of the obtained ZnO peaks indicate that the as-grown nanorods are highly crystalline with less impurities.

An individual ZnO nanorod is faceted as indicated in Fig. 3(b and c). The ZnO nanorod is highly crystalline, with a lattice spacing of about 0.26 nm, corresponding to the distance between adjacent (002) lattice planes. The selected-area electron diffraction (SAED) pattern confirms that the ZnO nanorod has a single crystalline structure and its growth direction is along the c-axis orientation, which corresponds to the (001) direction. It is in accordance with low index crystallographic face growth. In addition, the high-resolution transmission electron microscope (HR-TEM) image clearly shows the absence of stacking defects in the crystalline structure, which suggests that the crystals of individual rods are of good quality.

Fig. 4 shows the SEM images of the ZnO nanorod sample growing at different positions of the reaction kettle, whose interlining is made of teflon. ZnO nanorods grow at unwanted areas as shown in Fig. 4(a). During the growth reaction, ZnO powders are generated inside of the growth solution at the beginning of the growth, and then deposit onto the sample substrate as the ZnO growth seed,

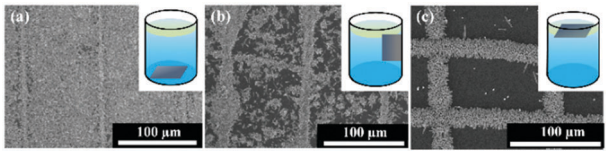

Fig. 4 SEM images of the ZnO nanorod growing sample (a) at the bottom, (b) at the sidewall and (c) upside-down at the top of the teflon-bottle. The insets are the corresponding schematic diagrams of the sample location.

which continues to grow ZnO nanorods. Temperature unevenness of the growth solution produces directional flow solution, and the patterned nanoparticle seeds move to the unpatterned (unseeded) adjacent substrate region due to the strong convective flow, which grows ZnO nanorods similarly. Based on the above two factors, growth of ZnO nanorods at the bottom of the reaction kettle is undesirable. Secondly, there is no ZnO nanopowder settlement to the sample at the sidewall in the reaction kettle, but the directional flow generated by the effect of the uneven temperature is still there, so the sample (Fig. 4(b)) is better than the sample at the bottom. Invert the sample at the top of the teflon-bottle kettle and let the seeded side of the substrate upside-down immersed in the growth solution. There will be no influence of the powder deposition as seeds and the directional flow of solution, so ZnO nanorods grow just at seeded areas (Fig. 4(c)). The ZnO nanorod array is greatly improved. So the position and the orientation of the ZnO precursor sample in the reactor play an important role in the growth of the ZnO nanorod array. The sample inverted on the top of the teflon-bottle is the ideal position and orientation, and the ZnO nanorod pattern is optimized.

At different growth stages, the lateral and axial surface growths are found to have different relative growth rates. During the first 10 hours (h), axial growth is more significant than lateral growth, as shown in Fig. 5(a and b). Due to the anisotropic crystal properties, the velocities of growth in different directions under hydrothermal conditions are $V_{[0001]} > V_{[0110]} > V_{[1000]}$.[28] The diameter of the individual ZnO nanorod decreases gradually from the bottom to the top exhibiting a tower-like shape. The initial seed layer can serve as heterogeneous nucleation sites and initiate a layer-by-layer growth

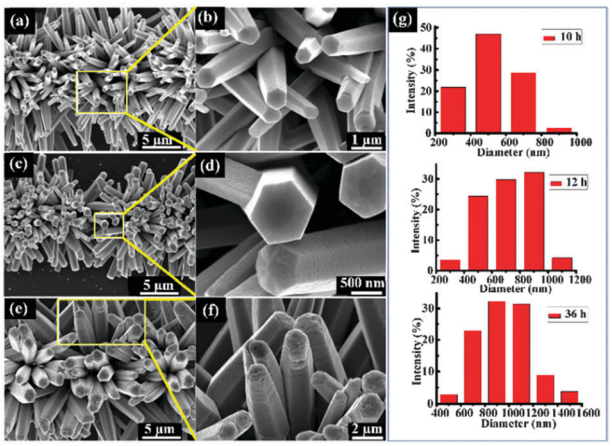

Fig. 5 SEM images of ZnO nanorods growing upside-down in the teflon-bottle at 90 °C for (a and b) 10 h; (c and d) 12 h; and (e and f) 36 h. (g) Histograms of ZnO nanorod top diameter distribution with different growth times.

along the *c*-axis, which results in the formation of tower-like nanorods.[29] Moreover, the side and top surfaces of nanorods are very smooth and clean. When the growth time exceeds 10 h, lateral growth is more significant than axial growth. The nanorods obviously increased in diameter but are always about 5–15 μm in length (Fig. 5(c–f)) when the growth time is from 10 to 36 h. The length of ZnO nanorods is almost independent of time, indicating little axial growth. The side and most of the top surfaces of the ZnO nanorods are very smooth and clean, while some of the top surfaces are observed to have protrusions but smooth (Fig. 5(d)) due to the beginning of erosion by the growth solution. During the period of 36 h (Fig. 5(e)), the ZnO nanorod diameter increases more slowly with the growth time of 36 h than that of ZnO nanorods growing for 12 h, and the top of the nanorods is subjected to erosion by the growth solution, and the shape becomes irregular (Fig. 5(f)).

The top diameter distributions of ZnO nanorods are presented in Fig. 5(g). More than 160 nanorods are tested in order to determine the diameter distribution. The quantitative analysis shows that the regions of top diameter distributions are enlarged and the average top diameters increase with increasing growth time from 10 h to 36 h. When the growth time is 10 h, the ZnO nanorods obtained have uniform diameters between 200–1000 nm, and the average top diameter is 520 nm with a standard deviation of 153 nm. The diameters of nanorods for a longer growth time (12 h) distribute in the range of 200–1200 nm with the average top diameter of 728 nm (±183 nm). However, the region of distribution with the growth time of 36 h ranges from 400 to 1600 nm, and the average top diameter is 962 nm (±214 nm).

Adjusting the process parameters, we have prepared a gas sensor of ZnO parallel arrays on the alumina substrate with the Ag interdigital electrode (Ag IDT), which is shown in Fig. 6(a). The current–voltage (*I–V*) characteristic (Fig. 6(b)) indicates that the electrical current is linearly proportional to the intensity of applied bias voltage (−10–10 V), which evidences that the ZnO sample has Ohmic behavior rather than diode-like behaviour. This is beneficial for gas sensing properties because the sensitivity of a gas sensor can be maximized when the metal–semiconductor junction has Ohmic behavior or a negligible junction resistance.

The ZnO sample is not suitable for use as a NO_2 sensor at room temperature,[30] but has good sensitivity to NO_2 at 225 °C. Fig. 6(c) shows dynamic responses of the ZnO sample to nitrogen dioxide (NO_2) gas at various concentrations from 1 to 100 ppm at 225 °C. The resistance increases instantaneously to a maximum, which is maintained at the maximum resistance upon exposure to NO_2 and recovered completely to the initial value upon the removal of NO_2. The response of the ZnO sample to NO_2 gas is stable and reproducible for the repeat test.

The corresponding sensitivities (*S*) are commonly given by the equation: $S = (R_g - R_a)/R_a$, where R_g is the resistance of the sample under a NO_2 atmosphere and R_a is the sample resistance under an air atmosphere. Fig. 6(d) shows the *S* of the ZnO sample versus NO_2 concentrations in the range of 1–100 ppm. The data of *S* have been fitted by least squares fitting. It is clearly seen that *S* increases from 1 to 88 with increasing concentration, and an approximately linear increase relationship between the corresponding sensitivities and NO_2 concentrations is observed

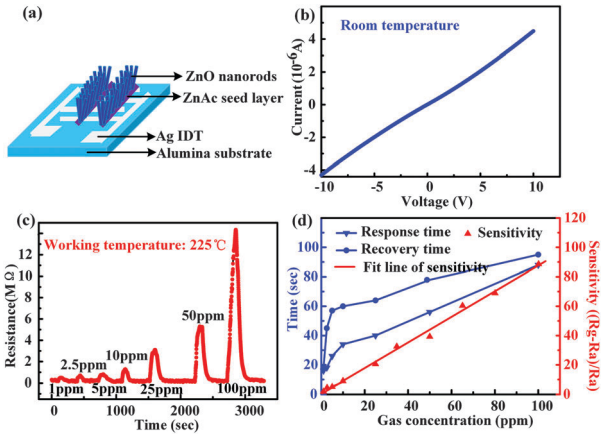

Fig. 6 (a) Schematics of the ZnO gas sensor. (b) Room-temperature *I–V* characteristic of a ZnO-nanorod gas sensor in an air atmosphere. (c) Dynamic responses of the ZnO sample to NO_2 gas. (d) Variation of sensitivities, response and recovery times of the ZnO sample at different concentrations of NO_2.

for the ZnO sample at the measured concentration. The response time is defined as the time taken by the sensor to attain 90% of the maximum increase in resistance on exposure to target gas and the recovery time as the time to get back 90% of the maximum resistance when exposed to clean air. The variations of response and recovery times with different concentrations of NO_2 are represented in Fig. 6(d). It is observed that the response and recovery times are both increased with respect to NO_2 concentration, and the increases slow down gradually when the gas concentrations increase. The response time increases from 16 s to 88 s while recovery time relatively ranges from 18 to 95 s with increasing NO_2 concentration from 1 to 100 ppm. This is expected for a reasonable sensor to recover in a short period of time to be prepared.

This communication presents selective growth of ZnO nanorods by a combination of MES and the low-temperature hydrothermal synthesis method, which is demonstrated to be an excellent method for patterned ZnO nanostructure array fabrication. By varying the printing conditions and the hydrothermal reaction time, the structure of the ZnO nanorod array can be fabricated in a low cost, low-temperature, template-free, environment-friendly, and highly controllable manner. High-density, radially grown, flower-type structures are clearly observed, and the distributions of these tower-like nanorods are uniform. *I–V* characteristics and sensing measurements indicate that the ZnO sample has a good Ohmic behavior and high response to oxidizing gas NO_2 at low concentrations (1–100 ppm) at 225 °C. Both response and recovery times are very fast for the ZnO sample exposed to NO_2 and clean air, respectively. These findings introduce new opportunities to obtain patterned nanostructure materials used in gas sensing. Similar methods can be applied to fabricate almost any patterned shapes and any seed-growing nanostructure materials.

The authors acknowledge supports from the National Natural Science Foundation of China (51322507, 51035002, 51421062) and the New Century Excellent Talents in University (NCET-11-0171).

Notes and references

1 D. Chandra, S. Mridha, D. Basak and A. Bhaumik, *Chem. Commun.*, 2009, 2384–2386.
2 M. Willander, O. Nur, Q. X. Zhao, L. L. Yang, M. Lorenz, B. Q. Cao, J. Z. Perez, C. Czekalla, G. Zimmermann, M. Grundmann, A. Bakin, A. Behrends, M. Al-Suleiman, A. El-Shaer, A. C. Mofor, B. Postels, A. Waag, N. Boukos, A. Travlos, H. S. Kwack, J. Guinard and D. L. Dang, *Nanotechnology*, 2009, **20**, 332001.
3 R. Zou, G. He, K. Xu, Q. Liu, Z. Zhang and J. Hu, *J. Mater. Chem. A*, 2013, **1**, 8445–8452.
4 W. Z. Xu, Z. Z. Ye, Y. J. Zeng, L. P. Zhu, B. H. Zhao, L. Jiang, J. G. Lu, H. P. He and S. B. Zhang, *Appl. Phys. Lett.*, 2006, **88**, 173506.
5 L. C. Chen, C. H. Tien, Y. M. Luo and C. S. Mu, *Thin Solid Films*, 2011, **519**, 2516–2519.
6 E. Lee, J. Ko, K. H. Lim, K. Kim, S. Y. Park, J. M. Myoung and Y. S. Kim, *Adv. Funct. Mater.*, 2014, **24**, 4689–4697.
7 R. Ahmad, N. Tripathy, D. U. J. Jung and Y.-B. Hahn, *Chem. Commun.*, 2014, **50**, 1890–1893.
8 G. Kiriakidis, I. Kortidis, S. D. Cronin, N. J. Morris, D. R. Cairns and K. A. Sierros, *Thin Solid Films*, 2014, **555**, 68–75.
9 S. Kim, C. H. Kim, S. K. Lee, J. H. Jeong, J. Lee, S. H. Jin, W. S. Shin, C. E. Song, J. H. Choi and J. R. Jeong, *Chem. Commun.*, 2013, **49**, 6033–6035.
10 F. Xu, Y. Lu, L. Sun and L. Zhi, *Chem. Commun.*, 2010, **46**, 3191–3193.
11 Y. C. Chen, C. H. Tu, Y. F. Lai, K. Y. Hsu and C. P. Liu, *J. Alloys Compd.*, 2013, **554**, 115–121.
12 L. Wang, X. Zhang, S. Zhao, G. Zhou, Y. Zhou and J. Qi, *Appl. Phys. Lett.*, 2005, **86**, 024108.
13 M. Wang, B. Zhao, S. Xu, L. Lin, S. Liu and D. He, *Chem. Commun.*, 2014, **50**, 930–932.
14 D. Polsongkram, P. Chamninok, S. Pukird, L. Chow, O. Lupan, G. Chai, H. Khallaf, S. Park and A. Schulte, *Physica B*, 2008, **403**, 3713–3717.
15 C. J. Chang, S. Hung, C. K. Lin, C. Y. Chen and E. H. Kuo, *Thin Solid Films*, 2010, **519**, 1693–1698.
16 M. Barret, S. Sanaur and P. Collot, *Org. Electron.*, 2008, **9**, 1093–1100.
17 L. V. Gambuzza, PhD thesis, Università degli Studi di CATANIA, 2014.
18 H. Shao, X. Qian and B. Huang, *Mater. Sci. Semicond. Process.*, 2007, **10**, 68–76.
19 H. W. Kang, J. Yeo, J. O. Hwang, S. Hong, P. Lee, S. Y. Han, J. H. Lee, Y. S. Rho, S. O. Kim, S. H. Ko and H. J. Sung, *J. Phys. Chem. C*, 2011, **115**, 11435–11441.
20 K. S. Han, S. H. Hong, K. I. Kim, J. Y. Cho, K. W. Choi and H. Lee, *Nanotechnology*, 2013, **24**, 045304.
21 A. N. Hattori and H. Tanaka, Annual Conference on Oxide-Based Materials and Devices V, San Francisco, CA, 2014.
22 J. Yeo, S. Hong, M. Wanit, H. W. Kang, D. Lee, C. P. Grigoropoulos, H. J. Sung and S. H. Ko, *Adv. Funct. Mater.*, 2013, **23**, 3316–3323.
23 N. Bu, Y. Huang, X. Wang and Z. Yin, *Mater. Manuf. Processes*, 2012, **27**, 1318–1323.
24 Y. Huang, X. Wang, Y. Duan, N. Bu and Z. Yin, *Soft Matter*, 2012, **8**, 8302–8311.
25 H. Liu, M. Li, O. Voznyy, L. Hu, Q. Fu, D. Zhou, Z. Xia, E. H. Sargent and J. Tang, *Adv. Mater.*, 2014, **26**, 2718–2724.
26 Y. Duan, Y. Huang, Z. Yin, N. Bu and W. Dong, *Nanoscale*, 2014, **6**, 3289–3295.
27 Y. Huang, Y. Duan, Y. Ding, N. Bu, Y. Pan, N. Lu and Z. Yin, *Sci. Rep.*, 2014, **4**, 5949.
28 H. Yang, Y. Song, L. Li, J. Ma, D. Chen, S. Mai and H. Zhao, *Cryst. Growth Des.*, 2008, **8**, 1039–1043.
29 F. Sun, X. Qiao, F. Tan, W. Wang and X. Qiu, *Appl. Surf. Sci.*, 2012, **263**, 704–711.
30 S. Özturk, N. Kilinc and Z. Z. Ozturk, *J. Alloys Compd.*, 2013, **581**, 196–201.

